Materials Science-Poland, 41(3), 2023, pp. 18-26
http://www.materialsscience.pwr.wroc.pl/
DOI: 10.2478/msp-2023-0032

Role of crystallographic orientation in material behaviour under nanoindentation: Molecular Dynamics study

Aneta Kurgan, Lukasz Madej*

AGH University of Krakow, Krakow, Poland

The mechanical properties of materials can be analysed under deformation conditions by various laboratory tests. However, such experimental investigations become extremely complicated and often even impossible at the lower length scales where the arrangement of the atomic planes is considered. In this case, computational materials science is a robust alternative to extend the capabilities of laboratory tests. Therefore, the molecular dynamics technique was selected in the current work to evaluate the role of the local grain crystallographic orientation during nanoindentation testing. A pure aluminium sample was selected as a case study. For the sake of clarity, two distinctively different crystallographic orientations cube {100}<001> and hard {110}<011> were investigated in a set of arrangements: monocrystalline, bicrystalline, and polycrystalline. The influence of the substrate and the neighbouring grains on the material response to local deformation was evaluated. The research used two types of indenters: spherical and sharp-tipped. Results obtained were analysed with respect to the arrangement of atoms and load-displacement curves. This research proved that the role of crystallographic orientation in material behaviour under nanoindentation should not be neglected during the interpretation of data from this test.

Keywords: *nanoindentation, molecular dynamics, simulations, spherical indenter, sharp tip indenter*

1. Introduction

As a result of its low density, aluminium (Al) and its alloys are commonly used materials in various lightweight applications. As such, they are often subjected to processing during metal-forming operations, like rolling, forging, or extrusion [1]. However, the higher the demand for final products with more sophisticated properties, the more fundamental research on alloy behaviour is required. Various aspects of aluminium behaviour are currently being studied during laboratory tests. The influence of temperature, strain rates, or deformation levels in elastic and plastic regimes is primarily investigated with the use of standard macroscopic plastometric tests [2–4]. However, when local material behaviour is of interest, then the micro- nano- or picoindentation tests are most often used [5, 6]. These tests have the capability to measure the load-displacement response during deformation at a small length scale and identify local material properties, including Young's modulus and nano-hardness [7]. It is also possible to identify the stress–strain characteristics of particular grains that can be further used in advanced full-field numerical simulations [8]. Unfortunately, many unexpected factors can affect the identified local material response significantly at this length scale. Particular attention has to be paid to the surface hardening during sample preparation stages, the parallel surface alignment with respect to loading directions, the selection of subsequent indentation locations, the selection of indentation load, or even the removal of the debris from the indenter tip's surface. Details about this test, along with its advantages and limitations, can be found in *Nanoindentation* by Fischer-Kripps [9]. Additionally, in Madej et al. [10], during the investigation of porous materials, the authors pointed out the role of the microstructure state directly under the indentation imprint, which can also significantly affect the test results.

Therefore, this research is focused on the evaluation of the material response from nano/picoindentation testing with respect to the grain orientations in the direct vicinity of the imprint. Computational material science capabilities were

* E-mail: lmadej@agh.edu.pl

© Aneta Kurgan and Lukasz Madej. 2023. This is an open access article distributed under the Creative Commons Attribution-NonCommercial-NoDerivatives 4.0 License. (http://creativecommons.org/licenses/by-nc-nd/4.0/)

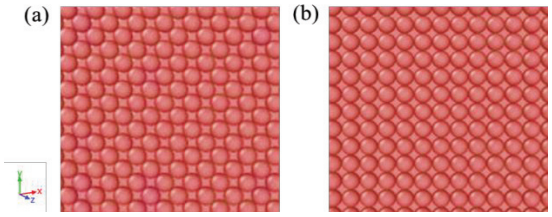


Fig. 1. Illustration of the atoms arrangement in (a) cube and (b) hard crystallographic orientations

employed during the research to improve a fundamental understanding of these mechanisms not affected by the real material heterogeneities nor the setup of the laboratory tests. The molecular dynamics (MD) technique was selected in the current work in particular to point out the role of the local grain crystallographic orientation during nano/picoindentation testing. The aluminium sample previously mentioned was selected as a case study. For the sake of clarity, two distinctively different crystallographic orientations, cube {100}<001> and hard {110}<011> (Figure 1), were investigated in a set of arrangements: monocrystalline, bicrystalline, and polycrystalline.

Generally, it is expected that when a load is applied to a single crystal, the atoms in the lattice will experience local forces and deformations. In a cube orientation, the crystal lattice has equal symmetry in all directions, which means that the atoms are arranged in a regular and symmetric manner. This arrangement allows for easier slip and movement of dislocations within the crystal lattice when an external load is applied. On the other hand, in a hard orientation, the crystal lattice has a specific direction that is less symmetric than the cube orientation. This means that the crystal structure is more resistant to deformation and dislocation movement compared to the cubic orientation. The presence of crystallographic planes or directions with low atomic packing densities can lead to increased resistance to slip and dislocation movement. Because of these differences in crystal structure and symmetry, monocrystals in hard orientations tend to exhibit higher strength and resistance to deformation compared to monocrystals in cube orientations. As a result of this increased resistance to slip and dislocation motion in hard orientations, higher forces are required to initiate plastic deformation.

2. Molecular dynamics model

Molecular dynamics [11–13] is a powerful tool for evaluating materials' behaviour and predicting their properties. MD is a well-established research tool in various fields, e.g., biology [14], chemistry [15], physics [16], and also materials science [17]. It is a computational technique that has the capability to evaluate direct atoms' and molecules' interactions over time. Therefore, MD simulations allow us to study the material's behaviour in great detail, including point, linear, and two- and three-dimensional defects like grain boundaries. As such, it provides an insight into the fundamental slip activities at particular crystalline planes.

Molecular dynamics is based on Newton's equation of motion [18, 19] in the following form:

$$F_i(t) = m_i \cdot \frac{d^2 r_i}{dt^2} \tag{1}$$

where: $F_i(t)$, the force acting on the i-th atom; m_i, the mass of the i-th atom; $\frac{d^2 r_i}{dt^2}$, the acceleration of the i-th atom; and $r_i = (x_i, y_i, z_i)$, the position of the i-th atom.

Then with the Verlet algorithm [20] and Taylor approximation [21], the position of the i-th atom is evaluated by means of the following formula:

$$r_i(t + \Delta t) = 2r_i(t) - r_i(t - \Delta t) + \frac{F_i(t)}{m_i}\Delta t^2 \tag{2}$$

where: r_i is the displacement of the i-th atom, t is the time, F_i is the force acting on the i-th atom, and m_i is the mass of the i-th atom.

The relationship between force and potential energy (U) is expressed as:

$$F_i = \frac{\partial U}{\partial r_i} \tag{3}$$

where: r_i is the displacement of the i-th atom, U is the potential energy, and F_i is the force acting on the i-th atom.

The key element of the MD model is the potential, which determines the interaction between

subsequent atoms. As a result, selecting the appropriate atomic potential is important in this procedure [22]. The embedded atom method (EAM) [23, 24] interatomic potential was selected for the current investigation with the parameters taken for the Al from available datasets [25].

The MD model was developed with the use of a large-scale atomic/molecular massively parallel simulator (LAMMPS) [26, 27] in 3D computational space to reflect the complexity of the real material behaviour, while initial atom arrangements in the samples were developed with Atomsk software [28, 29].

First, the unit cell of the sample atomic structure being investigated was selected. The face-centred cubic lattice (FCC) structure [30] was used for Al with a lattice constant equal to 4.02Å. To capture the sample constraints imposed by the surrounding material volume, a set of periodic boundary conditions was set on the side walls. A shrink-wrapped boundary condition was defined on the top surface, while the bottom surface was fixed. Based on such input data, a series of Al samples, namely, two monocrystals, two bicrystals, and three polycrystals, were generated with the Voronoi tessellation algorithm [31, 32]. The sample dimensions were the same and equal to $150 \times 150 \times 120$Å. At the same time, two crystallographic orientations representing the cube and hard orientations previously mentioned were assigned to monocrystalline and bicrystalline samples. The bicrystalline sample alignment is presented in Figure 2.

The baseline material behaviour under loading can be investigated with the presented monocrystalline sample alignment. At the same time, the bicrystalline samples allow studying the effect of the substrate on the applied indentation load.

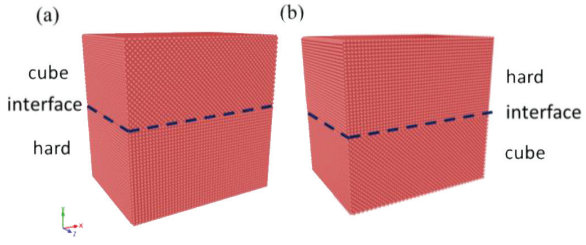


Fig. 2. Digital models (a) monocrystal in cube orientation, (b) monocrystal hard orientation, (c) bi-crystal in cube/hard arrangement, and (d) bi-crystal in hard/cube arrangement

The polycrystalline samples were also generated to investigate complex material behaviour under loading conditions. Three samples with five grains were constructed within the $150 \times 150 \times 150$Å computational domain, as seen in Figure 3.

The first two case studies were created on the basis of the cube and hard orientations. In each case, the central grain is in the cube Figure 3a or hard Figure 3b orientation. At the same time, the remaining grains represent the cube or hard orientations, respectively.

The last digital model of the sample (Fig. 3c) represents a fully random alignment of the grain's crystallographic orientations. In each case, the indentation was always carried out in the central grain during the simulation. As a result, the influence of the central grain neighbourhood can be clearly described.

As mentioned, two commonly used types of indenter tips were used during the investigation. The first is a sharp tip type indenter [33, 34], as presented in Figure 4a. This indenter imitates the shape of an inverted pyramid with a square base. The model was created on the basis of the carbon atoms with a diamond lattice and lattice parameter of 3.567Å. The second is a spherical type of indenter from Figure 4b. The sphere radius defines the size of this indenter and is equal to 20Å. In each case, the indenter speed was set as 2Å/femtosecond. Additionally, the spherical indenter and monocrystalline cube samples were used to evaluate the hardness value (7.14 GPa), to validate the model predictions against the experimental data presented by Liu et al. [35], and to successfully prove its robustness.

3. Results and Discussion

3.1. Nanoindentation using spherical indenter

Figure 5 shows the calculated indentation force-depth curves for the different types of cases investigated, namely monocrystalline, bicrystalline, and

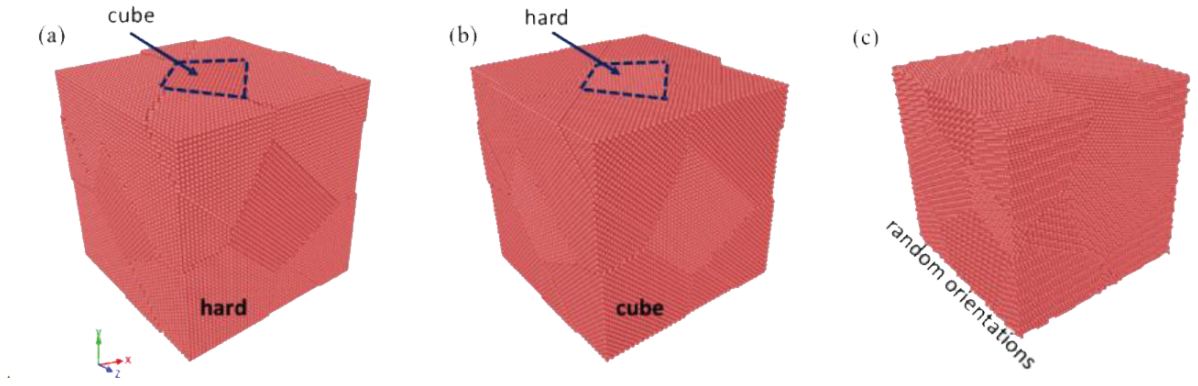


Fig. 3. Digital models: (a) central grain in a cube and others in hard orientations, (b) central grain in a hard and others in cube orientations, and (c) random grains orientations

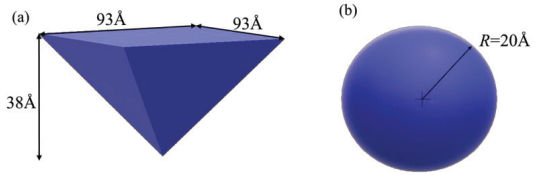


Fig. 4. Digital models of the indenter (a) sharp-tip and (b) spherical type

polycrystalline under spherical indenter loading conditions.

As seen in Figure 5a, up to a depth of 12.5Å, higher force values are recorded for the hard orientation, but at deeper depths the situation is reversed, which is unexpected behaviour that may be attributed to the pile-up developing faster for a softer material. In this case, the material around the indentation is displaced and pushed upwards, leading to an overestimation of the indent depth and also an increase in the surface contact between the tip and the material. In the case of the bicrystalline sample (Fig. 5b) this behaviour is not visible, and the forces for hard/cube are generally larger than cube/hard throughout the indentation. Serrated behaviour with clear oscillations is also more pronounced in the cube/hard sample case. A similar tendency is visible for the polycrystalline sample, with the central hard grain sample characterised by the highest force values. In this case, the sample with random grain orientation is most prone to deformation. The lower loads or strengths observed in the random polycrystalline sample (Fig. 5c) with respect to the other two hard/cube and cube/hard polycrystalline samples can be attributed to the collective behaviour of multiple grains and the interactions between dislocations and grain boundaries. The latter ones are interfaces between adjacent grains and introduce direct barriers to dislocation motion. It should also be pointed out that the size, distribution, and orientation of the grains within a polycrystalline sample can also influence its behaviour under loading.

A direct comparison of the forces recorded for indentation in the cube and hard grain in three investigated arrangements is shown in Figure 6. As expected, the bicrystalline sample provides the lowest force values. This is generally associated with the unconstrained deformation of the softer cube grains. At the same time, the monocrystalline sample provides the highest force values for both the cube and hard case. Interesting behaviour is also observed for the polycrystalline sample from Figure 6a, where the hard matrix directly constrains the deformation of the cube grain, leading to higher forces in the initial deformation stages with respect to the monocrystalline cube setup. Such a behaviour is not visible in the case of Figure 6b. Therefore, it can be seen that the force used during indentation is affected by both the substrate and the environment of the grain into which it was indented.

As mentioned, during these tests, an interesting serration phenomenon was observed with a decrease in force during indentation. It was

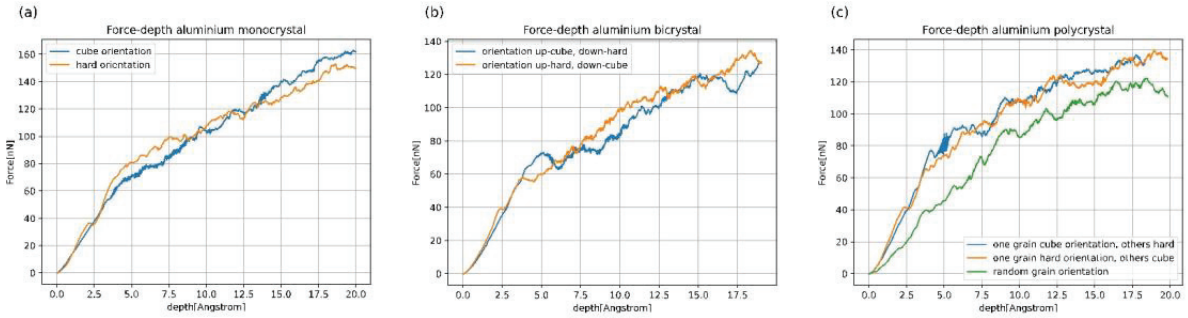


Fig. 5. Force-depth curves for (a) monocrystalline, (b) bicrystalline, and (c) polycrystalline samples for spherical indenter loading

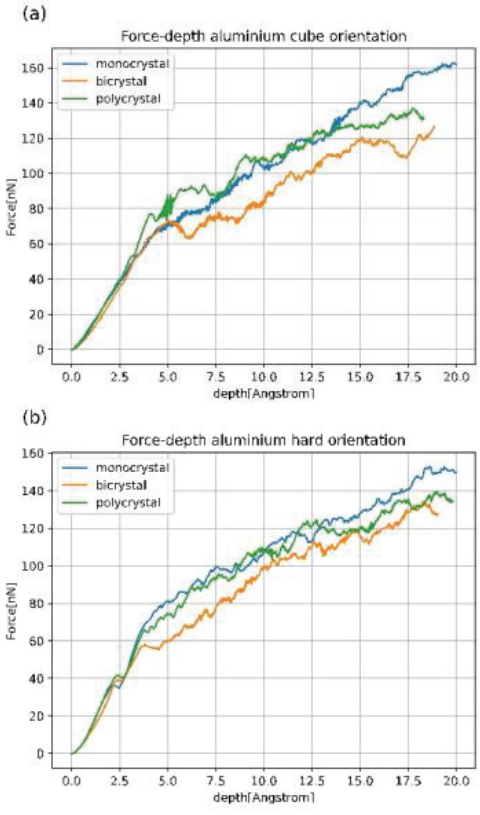


Fig. 6. Comparison of force-depth relation of monocrystalline, bicrystalline, and polycrystalline digital models during spherical indenter loading for (a) cube and (b) hard orientations

investigated with the example of the monocrystalline sample as a fundamental case study. Figure 7 represents the force drop for monocrystal with cube crystallographic orientation. The black circles mark the locations where the shift of atoms was noticed. They are described by slipping between atomic planes. It can be seen that the lines that are marked have become longer after the end of the drop in force. This means that there has been a slippage between the atomic planes, which is in line with the so-called pop-in event. During the initial stages of deformation, the applied load causes elastic deformation within the material; however, as the load continues to increase, dislocations nucleate and start moving. Finally, when a critical stress or load is reached, dislocations can move suddenly, and the dislocations "pop-in" into a new position or a slip plane occurs. This sudden dislocation movement rapidly increases displacement, causing the observed pop-in event in the load-displacement curve.

Figure 8 shows a similar force drop for the hard crystallographic orientation. This drop in force was relatively short, but the phenomenon of sliding between atomic planes could still be observed. The two stripes located on two parallel parts of the recess were noticed here. In the cross-section of the sample, some atoms moved downwards, but this time it was not in the form of a stripe.

3.2. Nanoindentation using sharp-tip indenter

Figure 9 shows the calculated indentation force-depth curves for similar cases, namely monocrystalline, bicrystalline, and polycrystalline samples, but for a sharp tip indentation.

In general, for the sharp-tip indentation, the material behaviour follows a clear relation, where

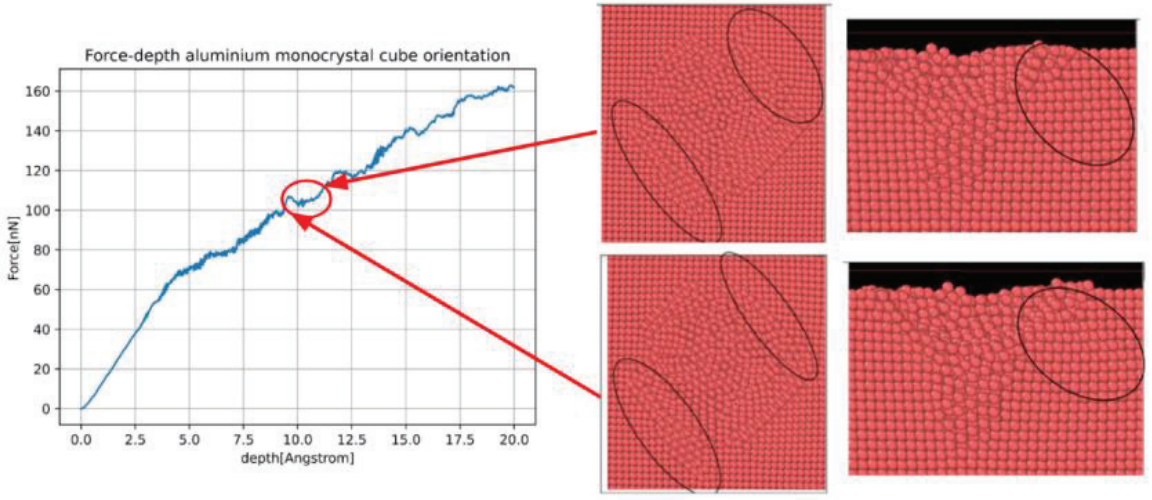


Fig. 7. Force drop analysis for monocrystal in cube orientation

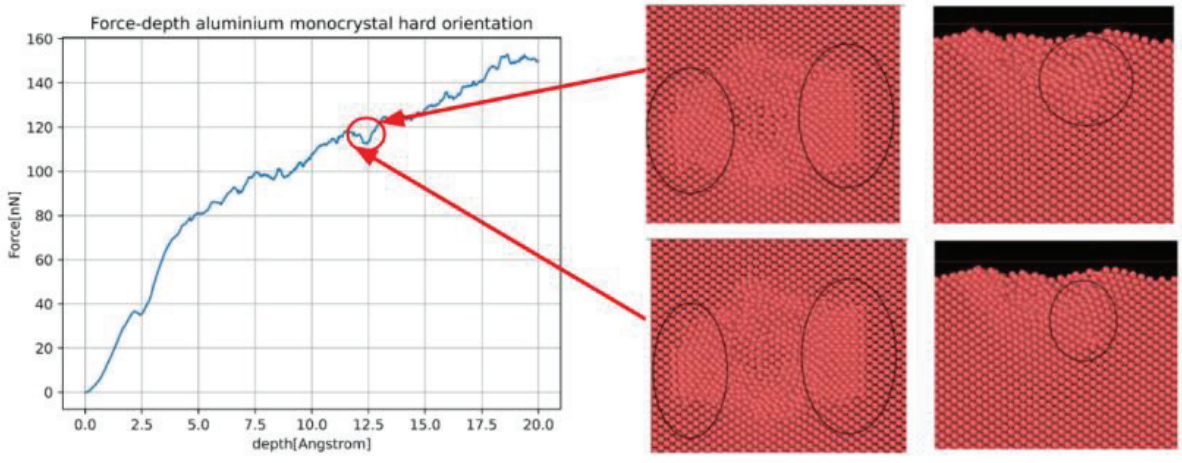


Fig. 8. Force drop analysis for monocrystal in hard orientation

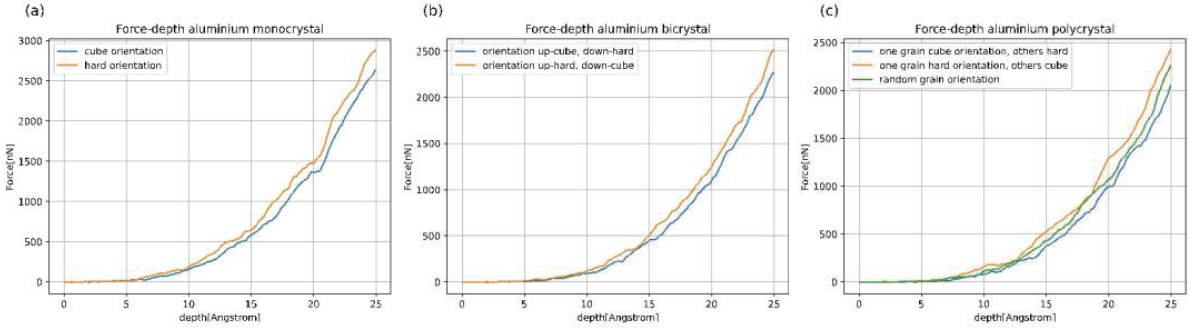


Fig. 9. Force-depth curves for (a) monocrystalline, (b) bicrystalline, and (c) polycrystalline samples for sharp tip indenter loading

the case studies with hard grains under direct loading led to higher force values during the test. At the same time, the serrations are less pronounced in this case, which can indicate a more uniform character of the slip activities. This is due to the fact that a sharp tip generates a high-stress concentration zone at the tip apex. As a result, a clearly localised deformation zone develops, which leads to plastic deformation in a smaller volume of material compared to a spherical tip. The high-stress concentration at the tip also facilitates the nucleation of dislocations during loading. Eventually, this concentrated deformation zone provides stability and prevents a laterally spreading deformation zone, which results in the serration seen in Figure 6. Again, a direct comparison of the forces recorded for indentation in the cube and hard grain in three arrangements is shown in Figure 10.

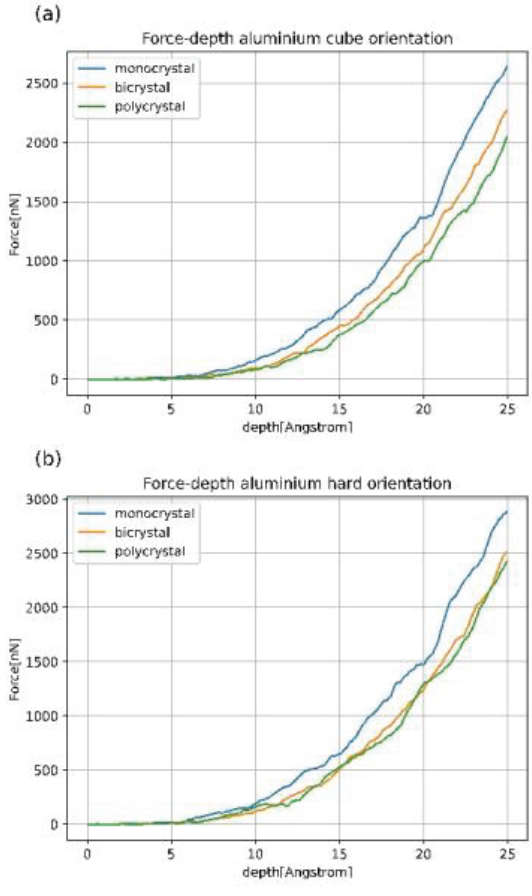


Fig. 10. Plots curve depth-force comparison of orientation for sharp tip indenter

As presented, the difference in force at a depth of 25Å between a monocrystal and a polycrystal can be quite large, approximately 500 nN, which again clearly points out the role of the matrix surrounding the grain under the indentation. Therefore, the nanoindentation should always be performed in a statistically relevant way. A series of indentations in different regions should minimise these grain-related variations and provide more representative results.

4. Conclusion

As presented, the molecular dynamics technique helped to evaluate the role of the local grain crystallographic orientation during the nanoindentation of the two distinctively different crystallographic orientations cube {100}<001> and hard {110}<011>. Based on the investigations with digital models representing monocrystalline, bicrystalline, and polycrystalline samples, the following conclusions can be drawn:

- The force used during indentation is affected by both the substrate and the environment of the grain into which it was indented.
- The size, distribution, and orientation of the grains within a polycrystalline material can influence direct barriers to dislocation motion.
- The serration phenomenon observed on curves of indentation with a spherical-type indenter is associated with slippage between the atomic planes.
- The sharp tip of the indenter generates a clearly localised deformation zone in comparison to the spherical tip.
- The role of the matrix surrounding the grain under the indentation cannot be neglected and should be taken into account during the interpretation of indentation data.

Conflict of interest

On behalf of both authors, the corresponding author states that there is no conflict of interest.

Data availability

The raw/processed data required to reproduce these findings cannot be shared at this time as the data also forms part of an ongoing study.

Compliance with ethical standards

Ethical approval: This article does not contain any studies with human participants or animals performed by any of the authors.

Acknowledgements

The financial assistance of the National Science Centre project No. 2019/35/B/ST8/00046 is acknowledged.

References

[1] Ji H, Ren K, Ding L, Wang T, Li JM, Yang J. Molecular dynamics simulation of the interaction between cracks in single-crystal aluminium. *Mater Today Commun.* 2022;30:103020.

[2] Liang Y, Qing L, Yu H, Huili Z, Yuxin W. Microstructure and mechanical properties of selective laser melted 18Ni300 steel. *Mater Sci-Poland.* 2022;40(3):64–71.

[3] Wang W, Xiao Y, Guo N, Min J. Finite element analysis of bipolar plate stamping based on a Yld2000 yield model. *Comput Methods Mater Sci.* 2022;22(1):7–12.

[4] Sabry I, Hewidy AM. Underwater friction-stir welding of a stir-cast AA6061-SiC metal matrix composite: optimization of the process parameters, microstructural characterization, and mechanical properties. *Mater Sci-Pol.* 2022;40(1):101–15.

[5] Gouldstone A, Chollacoop N, Dao M, Li J, Minor AM, Shen Y. Indentation across size scales and disciplines: Recent developments in experimentation and modelling. *Acta Mater.* 2007;55(12):4015–39.

[6] Świetlicki A, Walczak M, Szala M. Effect of shot peening on corrosion resistance of additive manufactured 17-4PH steel. *Mater Sci-Pol.* 2022;40(3):135–51.

[7] Tabor D. *The Hardness of Metals*. New York: Oxford University Press; 1951.

[8] Potts D, Axelsson K, Grande L, Schweiger H, Long M. *Guidelines for the use of advanced numerical analysis*. London: Thomas Telford Publishing; 2002.

[9] Fischer-Cripps A. *Nanoindentation*. New York: Springer-Verlag; 2004.

[10] Madej L, Legwand A, Setty M, Mojzeszko M, Perzynski K, Roskosz S, Chraponski J. Evaluation of capabilities of the nanoindentation test in the determination of flow stress characteristics of the matrix material in porous sinters. *Arch Civ Mech Eng.* 2022;22:21.

[11] Hansson T, Oostenbrink C, van Gunsteren W. Molecular dynamics simulations. *Curr Opin Struct Biol.* 2002;12:190–6.

[12] Hollingsworth SA, Dror RO. Molecular dynamics simulation for all. *Neuron.* 2018;99:1129–43.

[13] Wieczorek G, Niedzialek D. *Molecular dynamics*. Hoboken, NJ: John Wiley & Sons; 2020.

[14] Karplus M, McCammon JA. Molecular dynamics simulations of biomolecules. *Nat Struct Mol Biol.* 2002;9:646–52.

[15] van Gunsteren WF, Berendsen HJC. Computer simulation of molecular dynamics: methodology, applications, and perspectives in chemistry. *Angew Chem Int Ed.* 1990;29:992–1023.

[16] Shuichi N. Constant temperature molecular dynamics methods. *Prog Theor Phys Suppl.* 1991;103:1–46.

[17] Kus W, Mrozek A. Quantum-inspired evolutionary optimization of SLMoS2 two-phase structures. *Comput Methods Mater Sci.* 2022;22(2):67–78.

[18] Leimkuhler B, Matthews C. *Molecular dynamics: Interdisciplinary applied mathematics*. Berlin; Springer; 2015.

[19] Alonso-Blanco RJ, Muñoz-Díaz J. Newton's second law in field theory. *Differ Geom Appl.* 2021;79:101814.

[20] Martys NS, Mountain RD. Velocity Verlet algorithm for dissipative-particle-dynamics-based models of suspensions. *Phys Rev E.* 1999;59:3733–6.

[21] Abbasbandy S, Bervillier C. Analytic continuation of Taylor series and the boundary value problems of some nonlinear ordinary differential equations. *Appl Math Comput.* 2011;218:2178–99.

[22] Monk JD, Haskins JB, Bauschlicher CW, Lawson JW. Molecular dynamics simulations of phenolic resin: construction of atomistic models. *Polymer.* 2015;62:39–49.

[23] Daw MS, Baskes MI. Embedded-atom method: derivation and application to impurities, surfaces, and other defects in metals. *Phys Rev B.* 1984;29:6443–53.

[24] Daw MS, Baskes MI, Foiles MS. The embedded-atom method: a review of theory and applications. *Mater Sci Rep.* 1993;9:251–310.

[25] Mishin Y, Farkas D, Mehl M, Papaconstantopoulos D. Interatomic potentials for monoatomic metals from experimental data and ab initio calculations. *Phys Rev B.* 1998;59:3393–407.

[26] LAMMPS documentation. 21 Nov 2023 [Accessed on 2023/11/29]. Available via: https://docs.lammps.org/Manual.html

[27] Thompson PA, Aktulga HM, Berger R, Bolintineanu SD, Brown WM, Crozier PS, et al. LAMMPS—a flexible simulation tool for particle-based materials modeling at the atomic, meso, and continuum scales. *Comput Phys Commun.* 2022;271:108171.

[28] Atomsk. 2010 [Accessed on 2023/11/29]. Available via: https://atomsk.univ-lille.fr/doc.php

[29] Hirel P. Atomsk: A tool for manipulating and converting atomic data files. *Comput Phys Commun.* 2015;197:212–9.

[30] Lee KW, Lee SH, Noh KH, Park JY, Cho YJ, Kim SH. Theoretical and numerical analysis of the mechanical responses of BCC and FCC lattice structures. *J Mech Sci Technol.* 2019;33:2259–66.

[31] Du Q, Faber V, Gunzburger M. Centroidal voronoi tessellations: applications and algorithms. *SIAM Rev.* 1999;41:637–676.

[32] Falco S, Jiang J, De Cola F, Petrinic N. Generation of 3D polycrystalline microstructures with a conditioned Laguerre-Voronoi tessellation technique. *Comput Mater Sci.* 2017;136:20–8.

[33] Zong W, Wu D, Li Z. Strength dependent design method for the crystal orientation of diamond Berkovich indenter. *Mater Design.* 2016;89:1057–70.

[34] Zong WJ, Wu D, He CL. Radius and angle determination of diamond Berkovich indenter. *Measurement.* 2017;104:243–52.

[35] Luu H-T, Dang S-L, Hoang T-V, Gunkelmann N. Molecular dynamics simulation of nanoindentation in Al and Fe: on the influence of system characteristics. *Appl Surf Sci.* 2021;551:149221.

Received 2023-07-03
Accepted 2023-11-25